
Article:
Bryant, M orcid.org/0000-0003-4442-5169 and Neville, A (2017) Fretting corrosion of CoCr alloy: Effect of load and displacement on the degradation mechanisms. Proceedings of the Institution of Mechanical Engineers, Part H: Journal of Engineering in Medicine, 231 (2). pp. 114-126. ISSN 0954-4119

https://doi.org/10.1177/0954411916680237

Fretting Corrosion of CoCr Alloy: Effect of Load and Displacement on the Degradation Mechanisms

M.Bryant*, A. Neville

Institute of Functional Surfaces (iFS), School of Mechanical Engineering, University of Leeds, UK.

M.g.bryant@leeds.ac.uk

0113 343 2161

Abstract

Fretting-corrosion of medical devices is of growing concern yet the interactions between tribological and electrochemical parameters are not fully understood. Fretting-corrosion of CoCr alloy was simulated and the components of damage were monitored as a function of displacement and contact pressure. Free corrosion potential (E_{corr}), intermittent linear polarisation resistance (LPR) and cathodic potentiostatic methods were used to characterise the system. Interferometry was used to estimate material loss post rubbing. The fretting regime influenced the total material lost and the dominant degradation mechanism. At high contact pressures and low displacements, pure corrosion was dominant with wear and its synergies becoming more important as the contact pressure and displacement decreased and increased respectively. In some cases an antagonistic effect from the corrosion-enhanced wear contributor was observed suggesting that film formation and removal may be present. The relationship between slip mechanism and the contributors to tribocorrosion degradation is presented.

Keywords: fretting-corrosion, tribocorrosion, contact mechanics, CoCrMo alloy

Fretting Corrosion of CoCr Alloy: Effect of Load and Displacement on the Degradation Mechanisms

M.Bryant, A. Neville

Institute of Functional Surfaces (iFS), University of Leeds, UK.

Abstract

Fretting-corrosion of medical devices is of growing concern yet the interactions between tribological and electrochemical parameters are not fully understood. Fretting-corrosion of CoCr alloy was simulated and the components of damage were monitored as a function of displacement and contact pressure. Free corrosion potential (E_{corr}), intermittent linear polarisation resistance (LPR) and cathodic potentiostatic methods were used to characterise the system. Interferometry was used to estimate material loss post rubbing. The fretting regime influenced the total material lost and the dominant degradation mechanism. At high contact pressures and low displacements, pure corrosion was dominant with wear and its synergies becoming more important as the contact pressure and displacement decreased and increased respectively. In some cases an antagonistic effect from the corrosion-enhanced wear contributor was observed suggesting that film formation and removal may be present. The relationship between slip mechanism and the contributors to tribocorrosion degradation is presented.

Keywords: fretting-corrosion; tribocorrosion; contact mechanics; CoCrMo alloy

1. Introduction

Biomedical alloys typically owe their corrosion resistance to the formation of an inert thin protective oxide film resulting in very low corrosion rates [1]. In order for a material to form a passive film, the substrate must rapidly react with oxidising agents in the environment. When a passive alloy is utilised in tribological applications, depending on the contact mechanics and lubrication regimes, mechanical removal of the passive film can occur leaving the reactive substrate exposed to the environment. Rapid oxidation of the substrate usually occurs resulting in metal ions being liberated from the metallic substrate. This process is known as tribocorrosion and is not exclusive to biomedical application of passive alloys. An important subset of tribocorrosion is fretting-corrosion. This describes the degradation of a material subjected to both chemical dissolution and mechanical damage initiated by small amplitude motion, typically less than 150 µm [2]. Whilst the tribological mechanisms of fretting have been documented, the links between mechanical and chemical factors are not fully understood.

Because tribocorrosion describes both the mechanical removal of material as well as chemical degradation, it is important to appreciate and to identify the contribution of corrosion and wear to material loss. Uhlig, as cited by Mischler [3], was amongst the first to recognise the role wear and corrosion play on the degradation in fretting contacts. Uhlig demonstrated that material deterioration results from two distinct mechanisms; mechanical wear and wear-accelerated corrosion to produce a simple mechanistic model based on mass conservation as shown in Equation 1, where M_{mech} represents the volume of material removed by mechanical wear, M_{chem} is the material loss due to wear accelerated corrosion.

Uhlig's expression suggests that the components of the total material damage M_{mech} and M_{chem} can be easily isolated. It proposes that M_{mech} captures all damage that is related to the mechanical removal of material and M_{chem} represents the material loss due to intermittent depassivation – or wear enhanced corrosion. In fact it is more complicated than this and tribocorrosion material damage consists of material degradation mechanisms that will only occur as a result of having both wear and corrosion occurring together. For example, if we remove corrosion the mass loss will reduce more than M_{chem} alone due to the influence of corrosion on wear.

Considering this, the model proposed by Uhlig can be broken down further to detail information regarding the synergistic reactions [4], where M_{wear} is a pure mechanical component (mechanical wear in the absence of corrosion), M_{cw} is the synergy between corrosion and wear (corrosion-enhanced wear). M_{corr} is a pure chemical component and M_{wc} is the synergy between wear and corrosion (wear-enhanced corrosion) however is only electrochemical in nature.

$$M_{total} = M_{mech} + M_{chem} \quad (1)$$

$$M_{mech} = M_{wear} + M_{cw} \quad (1.1)$$

$$M_{chem} = M_{corr} + M_{wc} \quad (1.2)$$

Fretting-corrosion of medical devices is common at load-bearing metallic interfaces; prevalent in orthopaedic [5-7], cardiovascular [8-11] and dental devices [12-14]. Such phenomena have been reported in both experimental and clinical literature. Instances of fretting-corrosion at the modular taper interface have been reported clinically since the 1980's [15]. However interest in the degradation at this interface has been renewed due to the high number of failures due to soft tissue reactions associated with fretting corrosion at this interface [16,7]. Fretting-corrosion of cardiovascular devices has recently been highlighted, occurring at overlapping interfaces (either braided or overlapped stents) [8-10]. Considering the complications associated with stent material related issues, the lack of literature in this area is surprising.

Fretting-wear has received attention for a number of years [2], with huge advances in the understanding been made through the work of Vingsbo [17] and Fouvry et al [18,19]. Renewed interest in the fundamentals of fretting-corrosion of biomedical alloys has been seen. Whilst the mechanisms of fretting-corrosion are generally accepted [20,21,2] the relationship and synergy between the tribological and electrochemical factors are still debated. Swaminathan et al [22,23] demonstrated, for a simple point contact, that fretting corrosion is affected by material couples, normal load and the motion conditions at the interface providing correlations between electrochemical currents and the dissipated mechanical energy. A relationship between the 'inter-asperity distances', calculated using electrochemical and mechanical inputs, and load was developed. In addition to this Baxmann et al [16] demonstrated links between fretting parameters, as given by Fouvry et al [19], and semi-quantitative electrochemical data showing that potential transients are related to the interfacial slip mechanisms.

Typical contact stresses and environments experienced in biomedical devices vary depending on their application. Contact conditions are seen to vary from 9–1000 MPa and 1-120 µm [16,22,24,25]. It can also be appreciated that the contact pressures and displacements developed in the biomedical interfaces do not tend to be uniformly distributed [26]. This is typically the case for modular taper interfaces in which stress concentrations are typically seen at the proximal-medial and distal-lateral sections of the taper [26]. It can be expected that a complex distribution of different degradation mechanisms will be established about the interface as a function of contact pressure, displacement and contact compliance further supporting the need for fundamental mechanistic investigations.

Whilst progress is currently being made towards understanding the fretting-corrosion degradation mechanisms of passive alloys the links between tribological and corrosion processes, and the dominant degradation mechanisms, at the interfaces are not still understood. Whilst many of the modern tribocorrosion theories [27-29] link tribological theory with electrochemical outputs, the assumptions used to fit such models and unique factors associated with fretting make such models difficult to apply especially for Hertzian contact configurations in which a combination of stick and slip are established across the interface. Taking this into consideration and also the fact limited studies have quantified both mechanical and electrochemical mass losses, gaining an understanding of these interactions over different loadings and slip regimes is of great importance. This study therefore takes a simplified point contact model, investigate and quantify the interactions between wear and corrosion as a function of displacement and contact pressure through a systematic experimental approach. It will go further to identify the synergies present at the interface for CoCr alloys and develop relationships between established tribocorrosion and fretting parameters to demonstrate how the degradation mechanisms varies as a function of the interfacial mechanics. Considering that many biomedical systems will establish multiple contact conditions across their metal-metal interfaces, an understanding of the interactions between wear and corrosion is of great importance. CoCrMo-CoCrMo interfaces are found throughout orthopaedic, dental and vascular applications.

2. Materials and Methods

2.1. Materials

Wrought Low carbon CoCrMo plates and wrought Ø28 mm LC CoCrMo femoral heads were utilised in this study to achieve a Hertzian point contact configuration. Nominal material properties and composition of alloys used in this study can be found in Table 1. All surfaces were polished to a surface roughness (S_a) of 10 nm and cleaned an degreased using acetone and N_2 air dried.

In all cases 50mL of Phosphate Buffered Saline solution (pH = 7.4) was utilised. This was prepared using deionised water and high purity chemical reagents. All tests were maintained at 37±1 ˚C for the duration of the test through the use of a closed looped hot water recirculation system.

2.2. Fretting Tribometer

In order to investigate the interactions between wear and corrosion in CoCrMo-CoCrMo fretting contacts, a reciprocating electromechanical fretting tribometer was utilised (Figure 1). The lower CoCrmo disc specimen was placed into a delrin holder and secured via a retaining ring equipped with O-rings to provide a water tight seal. The CoCrMo ball was fixed in holder parallel to the CoCrMo plate. Care was taken during preparation and during testing to ensure that no contact between the upper specimen holder to avoid contribution to the electrochemical signal from the sample holder. Electrical connection was taken from ball and plate (Figure 1) resulting in the CoCrMo ball and CoCrMo plate becoming the net-working electrode (WE).

Reciprocating motion was applied to the CoCrMo ball provided by the electromechanical actuator. The tangential force (F_t) was measured via cylindrical force transducer mounted axially to the actuator and CoCrMo ball. The magnitude of reciprocating motion (δ_d) of the upper sample relative to the static plate was measured by means of a fibre optic sensor fixed in the holder mounted to the base of the fretting apparatus. Table 2 shows the contact parameters chosen in this study. These were purposely chosen to represent the spread of contact conditions typically observed in literature [16,22,24,25]. In this study, the ratio of programmed displacement (δ_d) to actual sliding at the interface (δ_s) was used as an indication of slip mechanisms based on criteria given in [19,30]

2.3. Electrochemical Measurements

In order to facilitate electrochemical measurements and quantify corrosion during fretting, a Ag/AgCl reference electrode (RE) and Pt counter electrode (CE) (Sure flow Redox, Thermo-Scientific, USA) was integrated into the fretting tribometer (Figure 1). The WE, RE and CE were electrochemically connected via a potentiostat (PGSTAT101, Metrohm, Switzerland). Free corrosion potential (E_{corr}) measurements were made throughout the test in order to obtain a semi-quantitative indication of the passivity of the CoCrMo couple. E_{corr} represents the instantaneous potential difference established between the WE and RE due to a charge separation realised by the resistive nature of the metal and interfacial electrochemical double layer to electron transfer. For passive materials, such as CoCrMo alloys, upon the onset of rubbing a shift of E_{corr} is typically seen in the cathodic direction associated. This is linked with increased corrosion rates.

In order to quantify the mass losses due to corrosion at equilibrium, intermittent linear resistance polarisation (LPR) measurements were taken every 300 seconds. An applied potential of ±0.02 V versus E_{corr} at a scan rate of 1 mV/sec was applied to the sample to yield a linear relationship between applied potential and current. Due the charge separation developed at an interface, a linear relationship between applied potential and current is typically seen within 20-50 mV of E_{corr}. Wagner and Traud, as referenced by Frankel et al [31], identified that the reactions occurring around E_{corr} are mixed potential reactions owing from the anodic and cathodic half-cell reactions. It widely accepted that applying a potential within this region, no permanent changes to the electrode surface will be incurred. These were then converted to mass losses via application of the Stern-Geary relationship [32] and Faraday's Law [33] (assuming Faraday's constant (F) = 96480 $Cmol^{-1}$, molar mass (M) = 54.07 $gmol^{-1}$ and valence (z) of 2.5 for stoichiometric dissolution of the alloy). In order to separate the contributions of non-mechanically induced corrosion, R_p measurements were taken prior to sliding to ascertain the passive corrosion rates and used as the baseline corrosion currents. The difference in R_p during fretting was taken as the wear-induced corrosion, assumed to be emanating from the central contact area.

The Stern-Geary (SG) coefficient (Equation 2) was estimated by conducting Tafel analysis during fretting tests for additional samples to avoid damaging the surfaces of interest. Potentiodynamic polarisation from was conducted from ± 0.2 V vs E_{corr} at 1 mV/Sec for each contact pressure at 50 µm of displacement amplitude. The SG coefficient was calculated as being 0.041, 0.051 and 0.047 for fretting tests conducted at P_{max} = 0.4, 0.6 and 1 GPa respectively. Due to the large number of samples required to obtain Tafel constants as a function of time, the SG coefficient was assumed to be constant throughout the test. The authors acknowledge that this assumption is a simplification to the system, but thought to be the most accurate way to determine corrosion

currents without extensive polarisation and damage to the surfaces. An example of the raw LPR and current vs time curves generated in each test is shown in Figure 2. In order to isolate the corrosive aspects of the degradation (Eq1.2), potentiostatic tests were conducted. Here the potential of the WE was held at -0.8 V vs Ag/AgCl for the duration of the test to inhibit any dissolution. At this potential and experimental conditions it is assumed that the sample is cathodically protected (CP) and the oxidation of Co and Cr and reduction of Cr_2O_3 will not occur according to Pourbaix [34]. This approach has been presented in literature as a method to separate electrochemical contributions during tribocorrosion [35].

Figure 3 outlines the tribocorrosion protocol adopted in this study. Samples were initially immersed in PBS solution for 500secs with a measurement of polarisation resistance taken every 300 seconds. At 500 seconds, cyclic motion was initiated for 3000 cycles at 1Hz. After this cyclic motion was ceased and the sample able to recover for a further 500 seconds. β_a & β_c are the anodic and cathodic Tafel constants respectively obtained from potentiodynamic polarisation.

$$SG = \frac{\beta_a \beta_c}{2.303(\beta_a + \beta_c)} \quad (2)$$

2.4. Surface Analysis

To evaluate the volume of material loss due to wear and corrosion during fretting tests vertical scanning interferometry (VSI) was conducted on the both the CoCrMo balls and plates. Prior to VSI analysis each plate and counterbody was cleaned using acetone. The volume loss due to wear and corrosion was computed and taken as the material loss across the mean zero plane of the surface. The total mass loss due to wear and corrosion was taken as the sum of the volume lost from the CoCrMo head and plate. Due to the duration of the test, and extremely passive nature of the alloys, general material loss was assumed to be negligible (i.e. from outside wear track). Any mass loss would not be detectable through gravimetric or VSI methods. Optical light microscopy (Leica, Milton Keynes, UK) was also conducted in order to observe surface changes and wear mechanisms attributed to the presence of fretting at CoCrMo contacts.

3. Results

3.1. Fretting Regimes

Figure 4 shows the VSI, optical light micrographs and F_t versus δ curves obtained for the varying displacement amplitudes at P_{max}= 1 GPa. It can be seen at 1 GPa and low displacement amplitudes (δ_d<20 µm) a partial-slip and mixed slip fretting conditions exist at the interface. Under partial-slip conditions (P_{max}= 1GPa, δ_d = 10 µm, Figure 4a), a closed F_t-δ_d is observed and the applied displacement is mainly accommodated by elastic deformation of the contact and apparatus compliance. Under mixed-slip conditions (P_{max}= 1 GPa, δ_d = 20 µm, Figure 4b) an elliptical shape of the F_t-δ_d is observed. This suggests that some degree of sliding at the interface is imposed onto the elastic deformation already present at the contact interface (i.e. the contact is now comprised of both elastic compliance and sliding). From the shape of the fretting curves it is thought slip regime is on the transition to gross slip conditions. At δ_d>20 µm (Figure 4c-d) a gross-slip fretting regime was observed. This is characterised by an open F_t-δ_d quasi-rectangular shaped loop indicating that sliding was dominant in the interface. For all contact pressures and displacements below 1 GPa a gross-slip fretting regime was seen. This is accompanied by an abrasive wear mechanism typified by cutting and plastic deformation of the surface within the contact area.

In literature the relationship between displacement amplitude (δ_d) and sliding amplitude (δ_s) has been discussed as a convenient method of indicating the transition through different fretting regimes. Figure 5 demonstrates the δ_s/ δ_d as a function of δ_d and contact pressure with the criteria for transition outlined by Fouvry et al [19], Baxmann et al [16] and Mohrbacher et al [36]. Although these studies present the transition values for different alloy couples there is good agreement between the δ_s/ δ_d ratio and the mechanisms of slip with our results and those reported in literature. This is further supported by the images presented in Figure 4. It can be seen that a mixed-slip condition only occurs at P_{max}= 1 GPa when δ_d is greater than 10 µm but less than 30 µm for

CoCrMo/CoCrMo contacts lubricated in PBS solution. No significant differences between mechanical fretting data were seen under assumed pure wear (cathodic protection) conditions.

3.2. Mass Loss Results

Figure 6 demonstrates the mass loss as a function of actual total sliding distance and contact pressure for CoCrMo contacts considering the δ_s/ δ_d established at the interface. In each case a linear increase in mass loss was seen with increasing sliding distance. It is interesting to note the increase in mass loss for the lower contact pressure. This is thought to arise from the fact that less motion is accommodated by elastic deformation of the contact at the lower pressures. It can be seen that similar rates exist at contact pressures of 0.6 and 1.0 GPa despite the different slip mechanisms being present at the interface (Figure 6). This suggests that different pathways to degradation exist at the interface also dependant on contact pressure.

A comparison between mass losses under free corrosion conditions (E_{corr}) and with the application of CP are shown in Figure 7. It can be seen in all cases, apart from 10 and 50 µm displacements at 1 GPa, that a reduction in mass loss can be observed when corrosion is removed from the degradation processes.

3.3. Electrochemical Response

Figure 8 demonstrates the E_{corr} as a function of time and associated VSI images for illustration. E_{corr} curves at δ_d = 10, 30 and 50 µm are only shown for clarity. In the case for passive alloys (ie those owing their corrosion resistance to the formation of an oxide film) a decrease in E_{corr} upon the onset of friction is an indication of the synergistic interactions present between wear and corrosion. It can be seen that the shift and magnitude of the E_{corr} in the cathodic direction (at t = 500 seconds) is predominantly governed by the slip mechanism and magnitude of δ_s. It is hypothesised that the decrease in E_{corr} is brought about by changing the ratio of Anodic:Cathodic areas resulting in a depolarisation of the anodic reaction in the cathodic direction and the establishment of a galvanic couple between active and passive areas on the metal [27].

3.4. Relative Contributions to Mass Loss

Utilising intermittent LPR measurements the total mass loss due to electrochemical chemical reactions (M_{corr}+M_{wc}) can be estimated. Figure 9 demonstrates the relative proportions of total mass loss attributed to M_{chem} (M_{corr}+M_{wc}) and M_{mech} (M_{wear}+M_{cw}) (assuming the density of the material = 8.5 g.cm^{-1}). For P_{max} = 0.4 GPa, it can be seen that as displacement increases, the mechanism of degradation also change. At P_{max}= 0.4 GPa δ_d = 10 µm, mass losses due to electrochemical processes was seen to account for 27 ± 17 % of the total mass loss. This proportion was seen to decrease with increasing δ_d. At P_{max} = 0.4 GPa δ_d = 50 µm, mass losses due to electrochemical reactions was seen to account for 11 ± 9 % of the total mass loss indicated that the mechanism of material loss had become a dominated by mechanical processes.

It is particularly interesting to note that when P_{max} = 0.6 GPa, the mass loss increased with increasing displacement amplitude whilst the relative contributions to mass loss remained similar. In all cases the mass loss due to electrochemical reactions accounted for 35 - 45 % of the total material loss. When P_{max} = 1 GPa, similar comparable mass losses were observed when P_{max} = 0.6 GPa. However material loss was predominantly due to corrosion. When P_{max} = 1 GPa δ_d = 10 µm, corrosion was seen to account for 92 % of all material loss. It was observed that as δ_d increased, the mass losses due to mechanical actions increased. When P_{max} = 1 GPa, δ_d = 50 µm electrochemical dissolution was seen to account for 65 % of all material lost. These increases in mechanical losses (M_{mech}) are thought to become more dominant as the fretting regime makes a transition from partial to mixed to gross slip fretting mechanisms.

4. Discussion

In this paper the effects of tribological parameters on the fretting-corrosion behaviour of CoCrMo-CoCrMo fretting couples has been examined. The aim of this paper was to evaluate the synergistic interactions between wear and corrosion and to understand how these vary with the contact conditions (ie load and nature of slip). The results have shown that the mechanism of slip and the load applied to the interface significantly affects the so called ‘pathways to degradation’ i.e. if the system is wear, corrosion or wear-corrosion dominated. Mass losses due to corrosion become dominant as the magnitude of δ_s/ δ_d and contact pressure decrease and increase

respectively. Using the formulation determined by Stack et al [38], the relationship between M_{chem}/M_{wear} provides a criterion for the dominant degradation regime present in a tribocorrosion system. The different degradation mechanisms are detailed in Table 3. Figure 10 demonstrates the variation in degradation mechanism as a function of δ_s/δ_d, as given by Fouvry et al [19] and initial contact pressure. It can be seen that the degradation mechanism transitions from a corrosion dominated degradation mechanism at high contact pressures and a partial-slip regime to a wear-corrosion dominated process at lower contact pressures and gross-slip conditions. This is the inverse when compared to macro sliding tests where a transition to a wear dominated regime is seen with increasing load as reported by Mathew et al [39]. The results presented in this paper further suggest that a contact condition exists where synergism can be maximised supporting other tribocorrosion studies [39].
The trends in material loss as a result of fretting regime have been well documented. Vingsbo and Söderberg [17] highlighted that mass loss rates decrease as normal load and displacement amplitude decrease. However this can be counteracted by low fatigue life when in partial slip regimes. Fouvry et al [18] further stated that the tangential amplitude, which controls the stress amplitudes and then the cracking process, strongly increases under partial slip until a transition tangential force is met and gross slip is achieved and bulk material is removed. For a fretting contact in an aqueous environment it can be seen that the contributions to mass loss due to chemical processes increase as a function of applied load due to contact elasticity and the formation of environment conducive to accelerated corrosion (i.e. crevice corrosion) reducing the prevalence of this synergy (i.e. corrosion becoming dominant). Whilst the overall mass losses are smaller, correlating with already published literature, electrochemical losses are seen to increase suggesting that material lost as particulates has decreased whilst ionic material losses increase at 1 GPa when compared to 0.6 GPa. This is particularly relevant in the biomedical area where metal ion related biological responses have been reported.

Using the method outlined in Table 3 only goes part of the way to identify the key contributor to mass loss. From equation 1 it can be seen that M_{mech} includes a component of corrosive damage (M_{cw}) making it difficult to fully identify and define mass loss contributions. Further breaking the system down into its components it can be seen that M_{cw} accounts for a significant proportion of mass loss which otherwise would be lumped into the M_{mech} term. Splitting into each component, pure wear accounted for ≈ 50 %, M_{CW} ≈ 30-35 % and M_{WC} ≈ 15-20 % of material loss at 0.4 GPa (Figure 11a). The contributions of each synergy were seen to vary as the contact pressure increased and tribological conditions varied at the interface. A decrease and increase in the mechanical and corrosion contributions, respectively, becomes evident as contact pressure increases to 0.6 GPa (Figure 11b) with M_{cw} becoming dominant at higher displacements. Pure wear components reduced when compared 0.4 GPa due to the decrease in sliding at the interface due to elastic compliance of the contact (as discussed above). This may be due to increase roughness of the surface due to the increased contribution of M_{wc} further demonstrating the importance of decoupling the degradation modes. At P_{max} = 1 GPa (Figure 11c), pure wear was seen to account for 15 % at δ_d = 10 µm to 40 % at δ_d = 50 µm of the total mass loss. Wear enhanced corrosion was seen to remain similar for each displacement accounting for 35-40 % of the total mass loss. Interestingly a negative or antagonistic synergy was observed only in the cases at 1 GPa, accounting for -50 % to -20 % depending upon the displacement applied. This was seen to decrease (i.e. less antagonistic) with increasing displacement.

As the contact transitions into a gross slip regime, interesting variations in the M_{wear}, M_{wc} and M_{cw} could be observed (Figure 12). A seemingly exponential increasing behaviour was seen for each of the contributors as a function of the δ_s/δ_d. These were seen to transition at a $\delta_s/\delta_d \approx 0.9$. This may be explained as the transition from fretting to reciprocating wear in which rapid increases in wear will be expected with increasing sliding distance. The antagonistic effect of M_{cw} diminishes and a transition to positive synergy can be observed with decreasing contact pressure and increased sliding at the interface (Figure 12c). It is commonly hypothesised that this negative synergy is a result of the formation of a protective film at the contact due to electrochemical reactions [40]. Whilst in this study no attempt was made to quantify the chemical compositions, negative synergy could be achieved a number of ways in a fretting-corrosion contact. These can be the formation of corrosion product within the contact (i.e. compacted oxides) [41] both reducing corrosion and the progression of wear through mechanical alterations to the surface/subsurface or electrochemically affected fatigue due to increase reduction of H^+ at the near interface affecting local mechanical properties. The links between the fatigue life and slip mechanisms have been demonstrated by Vingsbo and Söderberg [17]. Materials have been shown to be

susceptible to fatigue like behaviour under stick conditions. Whilst fatigue is generally consisted a time dependent phenomena, under these circumstances H^+ is being reduced at a higher rate due to the imposed over-potential. It could therefore be expected that H^+ may ingress into the uppermost of the surfaces, modifying the local mechanical properties of the material. At a time scale sufficiently short enough to resist subsurface crack formation and propagation, localised changes in the local mechanical properties may be beneficial in reducing overall mass loss due to increase hardness however will be subject to further investigation.

4.1. Summary

Recently a number of studies have presented correlations between tribological contact parameters and fretting corrosion characteristics of materials typically used in biomedical applications. This paper goes further to quantify the individual contributors to mass loss using well established concepts. The influence of slip regime on the wear rate was first presented by Vingsbo and Söderberg [17]. They demonstrated that as the contact pressure and displacement increased, a decrease and increase in the fretting wear rate could be observed respectively. This is similar to the findings presented in this study with results following a similar response. Findings presented in this paper also complement those of Baxmann et al [16] who presented findings for Ti alloy tribo-couples. They demonstrated that a between existed between the electrochemical and mechanical factors demonstrating the magnitude of E_{corr} drop was related to the sliding amplitude and applied load. This study compliments the study of Baxmann by further demonstrating that although wear of the surfaces can be reduced by achieving low displacements and high contact pressures, the magnitude of corrosion can be increased for CoCrMo tribo-couples; this finding is particularly important in the context of medical devices were metal ions can elicit soft tissue responses. Baxmann concluded that by achieving relatively low micro-motions and sufficiently high contact pressures fretting-corrosion will be minimised. Whilst the use of high contact pressures and low displacements may reduce the synergy between wear and corrosion, long term implications such as corrosion assisted fatigue and hydrogen embrittlement may be promoted [42].

In the biological environment the co-existence of wear and corrosion in mated and loaded contacts is inevitable and unavoidable. It is therefore important to understand the degradation between the tribocorrosion mechanisms in order to effectively engineer the interfaces to provide optimal performance. This study has demonstrated that corrosion becomes dominant at high contact pressure and low displacements due to the elastic compliance within the contact resulting in limited slip at the interface. This reduces the synergy between wear and corrosion by reducing the volume of oxide abraded; however may leave the interfaces susceptible to fatigue as time progresses. As the contact pressure decreases it can be seen that wear becomes dominant, although corrosion is never truly eliminated. It can be appreciated that very different engineering solutions will be needed to address these different contact scenarios. Future work in this area will be focussed on understanding the mechanisms of degradation in mixed metal pairs and the evaluation of surface engineering processes for reduced wear and corrosion.

References

1. Hodgson, A., Kurz, S., Virtanen, S., Fervel, V., Olsson, C., Mischler, S.: Passive and transpassive behaviour of CoCrMo in simulated biological solutions. Electrochemica Acta **49**, 2167-2178 (2004).

2. Waterhouse, R.B.: Fretting Corrosion. International series of monographs on materials science and technology, Pergamon press, Cambridge, UK, (1972)

3. Mischler, S.: Triboelectrochemical techniques and interpretation methods in tribocorrosion: A comparative evaluation. Tribology International **41**(7), 573-583 (2008). doi:http://dx.doi.org/10.1016/j.triboint.2007.11.003

4. Watson, S.W., Friedersdorf, F.J., Madsen, B.W., Cramer, S.D.: Methods of measuring wear-corrosion synergism. Wear **2**(0), 476-484 (1995). doi:doi: 10.1016/0043-1648(95)90161-2

5. Goldberg, L., Gilbert, J.: In Vitro Corrosion Testing of Modular Hip Tapers. J Biomed Mater Res Part B **64B**, 79-93 (2003).

6. Bolland, B.J.R.F., Culliford, D.J., Langton, D.J., Millington, J.P.S., Arden, N.K., Latham, J.M.: High failure rates with a large-diameter hybrid metal-on-metal total hip replacement: clinical, radiological and retrieval analysis. Journal of Bone & Joint Surgery, British Volume **93-B**(5), 608-615 (2011). doi:10.1302/0301-620x.93b5.26309

7. Cook, R.B., Bolland, B.J.R.F., Wharton, J.A., Tilley, S., Latham, J.M., Wood, R.J.K.: Pseudotumour Formation Due to Tribocorrosion at the Taper Interface of Large Diameter Metal on Polymer Modular Total Hip Replacements. The Journal of Arthroplasty **28**(8), 1430-1436 (2013). doi:http://dx.doi.org/10.1016/j.arth.2013.02.009

8. Halwani, D.O., Anderson, P.G., Brott, B.C., Anayiotos, A.S., Lemons, J.E.: Clinical device-related article surface characterization of explanted endovascular stents: Evidence of in vivo corrosion. Journal of Biomedical Materials Research Part B: Applied Biomaterials **95B**(1), 225-238 (2010). doi:10.1002/jbm.b.31698

9. Kapnisis, K., Constantinides, G., Georgiou, H., Cristea, D., Gabor, C., Munteanu, D., Brott, B., Anderson, P., Lemons, J., Anayiotos, A.: Multi-scale mechanical investigation of stainless steel and cobalt–chromium stents. Journal of the Mechanical Behavior of Biomedical Materials **40**(0), 240-251 (2014). doi:http://dx.doi.org/10.1016/j.jmbbm.2014.09.010

10. Kapnisis, K.K., Halwani, D.O., Brott, B.C., Anderson, P.G., Lemons, J.E., Anayiotos, A.S.: Stent overlapping and geometric curvature influence the structural integrity and surface characteristics of coronary nitinol stents. Journal of the Mechanical Behavior of Biomedical Materials **20**(0), 227-236 (2013). doi:http://dx.doi.org/10.1016/j.jmbbm.2012.11.006

11. Zarins, C.K., Arko, F.R., Crabtree, T., Bloch, D.A., Ouriel, K., Allen, R.C., White, R.A.: Explant analysis of AneuRx stent grafts: relationship between structural findings and clinical outcome. Journal of Vascular Surgery **40**(1), 1-11 (2004). doi:http://dx.doi.org/10.1016/j.jvs.2004.03.008

12. Gao, S.S., Zhang, Y.R., Zhu, Z.L., Yu, H.Y.: Micromotions and combined damages at the dental implant/bone interface. International Journal of Oral Science **4**(4), 182-188 (2013).

13. Kang, T., Huang, S.Y., Huang, J.J., Li, Q.H., Diao, D.F., Duan, Y.Z.: The effects of diamond-like carbon films on fretting wear behavior of orthodontic archwire-bracket contacts. Journal of Nanoscience and Nanotechnology **15**(6), 4641-4647 (2015).

14. Rodrigues, D.C., Valderrama, P., Wilson, T.G., Palmer, K., Thomas, A., Sridhar, S., Adapalli, A., Burbano, M., Wadhwani, C.: Titanium corrosion mechanisms in the oral environment: A retrieval study. Materials **6**(11), 5258-5274 (2013).

15. Piehler, H.R., Portnoff, M.A., Sloter, L.E., Vegdahl, E.J., Gilbert, J.L., Weber, M.J.: CORROSION-FATIGUE PERFORMANCE OF HIP NAILS: THE INFLUENCE OF MATERIALS SELECTION AND DESIGN. In: ASTM Special Technical Publication 1985, pp. 93-104

16. Baxmann, M., Jauch, S.Y., Schilling, C., Blömer, W., Grupp, T.M., Morlock, M.M.: The influence of contact conditions and micromotions on the fretting behavior of modular titanium alloy taper connections. Medical Engineering & Physics **35**(5), 676-683 (2013). doi:http://dx.doi.org/10.1016/j.medengphy.2012.07.013

17. Vingsbo, O., Söderberg, S.: On fretting maps. Wear **126**(2), 131-147 (1988). doi:http://dx.doi.org/10.1016/0043-1648(88)90134-2

18. Fouvry, S., Kubiak, K.: Development of a fretting–fatigue mapping concept: The effect of material properties and surface treatments. Wear **267**(12), 2186-2199 (2009). doi:http://dx.doi.org/10.1016/j.wear.2009.09.012

19. Fouvry, S., Kapsa, P., Vincent, L.: Description of fretting damage by contact mechanics. ZAMM - Journal of Applied Mathematics and Mechanics / Zeitschrift für Angewandte Mathematik und Mechanik **80**(S1), 41-44 (2000). doi:10.1002/zamm.20000801311

20. Barril, S., Mischler, S., Landolt, D.: Electrochemical effects on the fretting corrosion behaviour of Ti6Al4V in 0.9% sodium chloride solution. Wear **259**(1–6), 282-291 (2005). doi:http://dx.doi.org/10.1016/j.wear.2004.12.012

21. Barril, S., Debaud, N., Mischler, S., Landolt, D.: A tribo-electrochemical apparatus for in vitro investigation of fretting–corrosion of metallic implant materials. Wear **252**(9–10), 744-754 (2002). doi:http://dx.doi.org/10.1016/S0043-1648(02)00027-3

22. Swaminathan, V., Gilbert, J.L.: Fretting corrosion of CoCrMo and Ti6Al4V interfaces. Biomaterials **33**(22), 5487-5503 (2012). doi:http://dx.doi.org/10.1016/j.biomaterials.2012.04.015

23. Swaminathan, V., Gilbert, J.L.: Potential and frequency effects on fretting corrosion of Ti6Al4V and CoCrMo surfaces. Journal of Biomedical Materials Research Part A **101A**(9), 2602-2612 (2013). doi:10.1002/jbm.a.34564

24. Gill, I.P.S., Webb, J., Sloan, K., Beaver, R.J.: Corrosion at the neck-stem junction as a cause of metal ion release and pseudotumour formation. Journal of Bone & Joint Surgery, British Volume **94-B**(7), 895-900 (2012). doi:10.1302/0301-620x.94b7.29122

25. Lanting, B.A., Teeter, M.G., Vasarhelyi, E.M., Ivanov, T.G., Howard, J.L., Naudie, D.D.R.: Correlation of Corrosion and Biomechanics in the Retrieval of a Single Modular Neck Total Hip Arthroplasty Design: Modular Neck Total Hip Arthroplasty System. The Journal of Arthroplasty **30**(1), 135-140 (2015). doi:http://dx.doi.org/10.1016/j.arth.2014.06.009

26. Zhang, T., Harrison, N.M., McDonnell, P.F., McHugh, P.E., Leen, S.B.: A finite element methodology for wear–fatigue analysis for modular hip implants. Tribology International **65**(0), 113-127 (2013). doi:http://dx.doi.org/10.1016/j.triboint.2013.02.016

27. Papageorgiou, N., Mischler, S.: Electrochemical Simulation of the Current and Potential Response in Sliding Tribocorrosion. Tribology Letters **48**(3), 271-283 (2012). doi:10.1007/s11249-012-0022-9

28. Vieira, A.C., Rocha, L.A., Papageorgiou, N., Mischler, S.: Mechanical and electrochemical deterioration mechanisms in the tribocorrosion of Al alloys in NaCl and in NaNO3 solutions. Corrosion Science **54**, 26-35 (2012). doi:http://dx.doi.org/10.1016/j.corsci.2011.08.041

29. Papageorgiou, N., von Bonin, A., Espallargas, N.: Tribocorrosion mechanisms of NiCrMo-625 alloy: An electrochemical modeling approach. Tribology International **73**, 177-186 (2014). doi:http://dx.doi.org/10.1016/j.triboint.2014.01.018

30. Oladokun, A., Pettersson, M., Bryant, M., Engqvist, H., Persson, C., Hall, R., Neville, A.: Fretting of CoCrMo and Ti6Al4V alloys in modular prostheses. Tribology - Materials, Surfaces & Interfaces **0**(0), 1751584X1751515Y.0000000014. doi:doi:10.1179/1751584X15Y.0000000014

31. G.Frankel, H.Isaacs, J.Scully, J.Sinclair: Wagner-Traud to Stern-Geary; Development of Corrosion Kinetics, in Corrosion Retrospective,. Journal of Electrochemical Society (2002).

32. M.Stern, Geary, A.L.: Electrochemical Polarization. Journal of the Electrochemistry Society **104**(1), 56-63 (1957).

33. M.Fontanna, N.Greene: Corrosion Engineering. Mc Graw Hill, New York (1978)

34. Pourbaix, M.: Atlas of electrochemical equilibria in aqueous solutions, 2d English ed ed. National Association of Corrosion Engineers., Houston, Tex (1974)

35. Yan, Y., Neville, A., Hesketh, J., Dowson, D.: Real-time corrosion measurements to assess biotribocorrosion mechanisms with a hip simulator. Tribology International **63**, 115-122 (2013). doi:http://dx.doi.org/10.1016/j.triboint.2012.08.006

36. Mohrbacher, H., Blanpain, B., Celis, J.P., Roos, J.R.: The influence of humidity on the fretting behaviour of PVD TiN coatings. Wear **180**(1–2), 43-52 (1995). doi:http://dx.doi.org/10.1016/0043-1648(94)06538-1

37. Kurtz, S.M., Kocagöz, S.B., Hanzlik, J.A., Underwood, R.J., Gilbert, J.L., MacDonald, D.W., Lee, G.-C., Mont, M.A., Kraay, M.J., Klein, G.R., Parvizi, J., Rimnac, C.M.: Do Ceramic Femoral Heads Reduce Taper Fretting Corrosion in Hip Arthroplasty? A Retrieval Study. Clinical Orthopaedics and Related Research **471**(10), 3270-3282 (2013). doi:10.1007/s11999-013-3096-2

38. Stack, M.M., Chi, K.: Mapping sliding wear of steels in aqueous conditions. Wear **255**, 456-465 (2003).

39. Mathew, M.T., Runa, M.J., Laurent, M., Jacobs, J.J., Rocha, L.A., Wimmer, M.A.: Tribocorrosion behavior of CoCrMo alloy for hip prosthesis as a function of loads: A comparison between two testing systems. Wear **271**(9–10), 1210-1219 (2011). doi:http://dx.doi.org/10.1016/j.wear.2011.01.086

40. Wood, R.J.: Tribo-corrosion of coatings: a review. Journal of Physics D: Applied Physics **40**(18), 5502 (2007).

41. Feng, I., Barrans, S.: An experimental study of fretting. Proceedings of the Institution of Mechanical Engineers **170**(1), 1055-1064 (1956).

42. Rodrigues, D.C., Urban, R.M., Jacobs, J.J., Gilbert, J.L.: In vivo severe corrosion and hydrogen embrittlement of retrieved modular body titanium alloy hip-implants. Journal of Biomedical Materials Research Part B: Applied Biomaterials **88B**(1), 206-219 (2009). doi:10.1002/jbm.b.31171

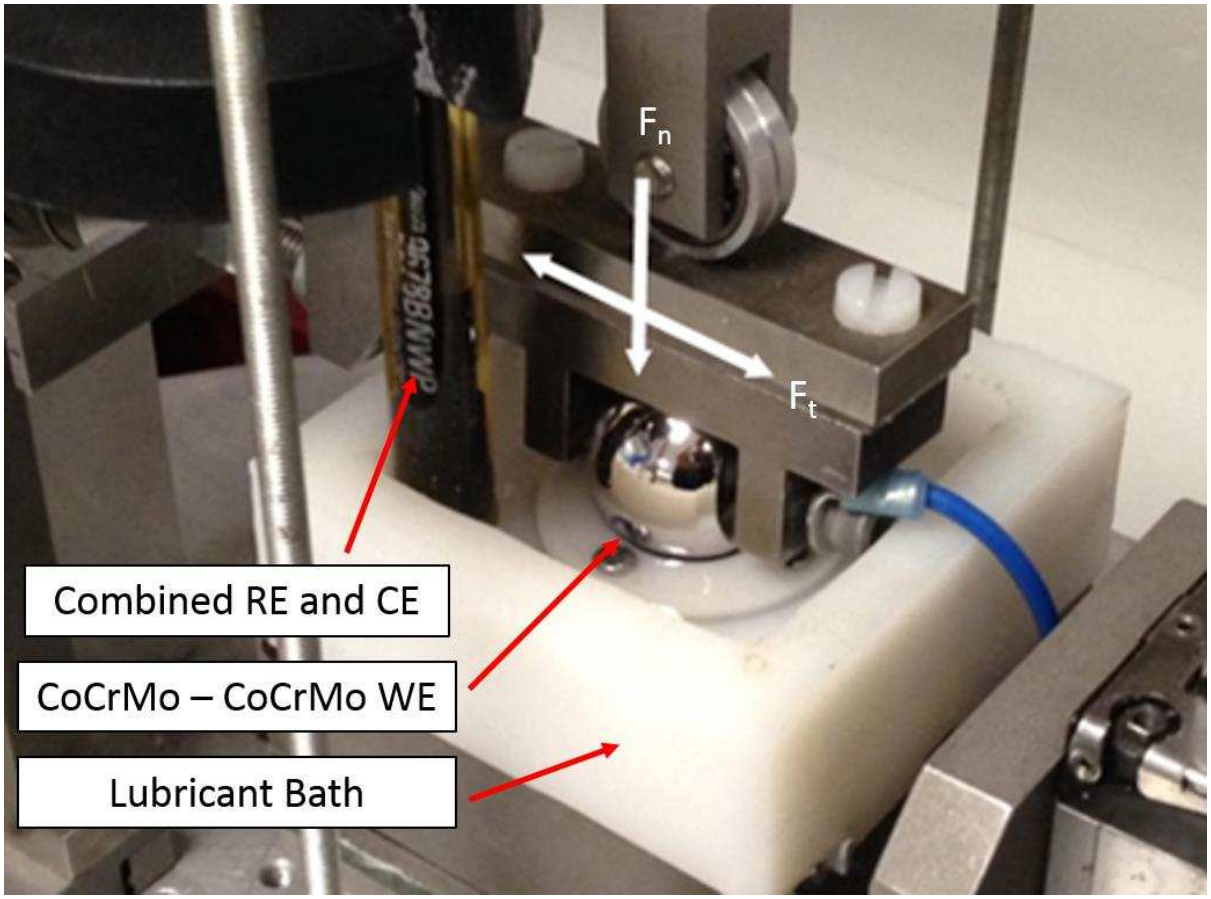

Fig. 1 Overview of ball on plate configuration.

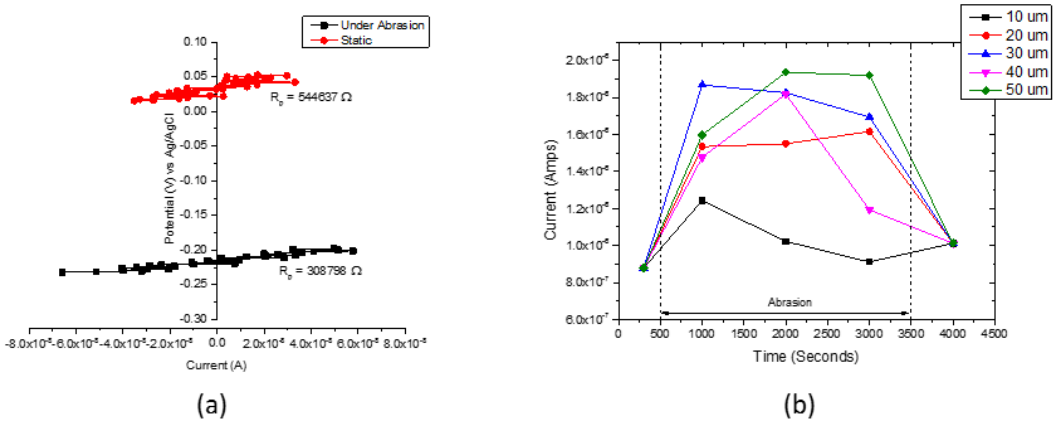

Fig. 2 – Example of a) linear resistance polarisation (LPR) measurements under static and abrasion conditions and b) current (obtained from LPR data) evolution as a function of test duration.

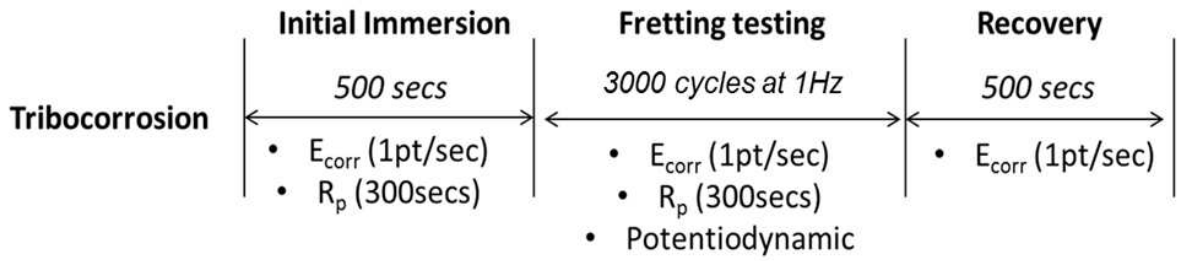

Fig. 3 Tribocorrosion protocol adopted in this study under free corrosion conditions. For cathodicaly protected tests, the sample was held at -0.8V versus Ag/AgCl for the entirety of the test. The same immersion and fretting testing times were used.

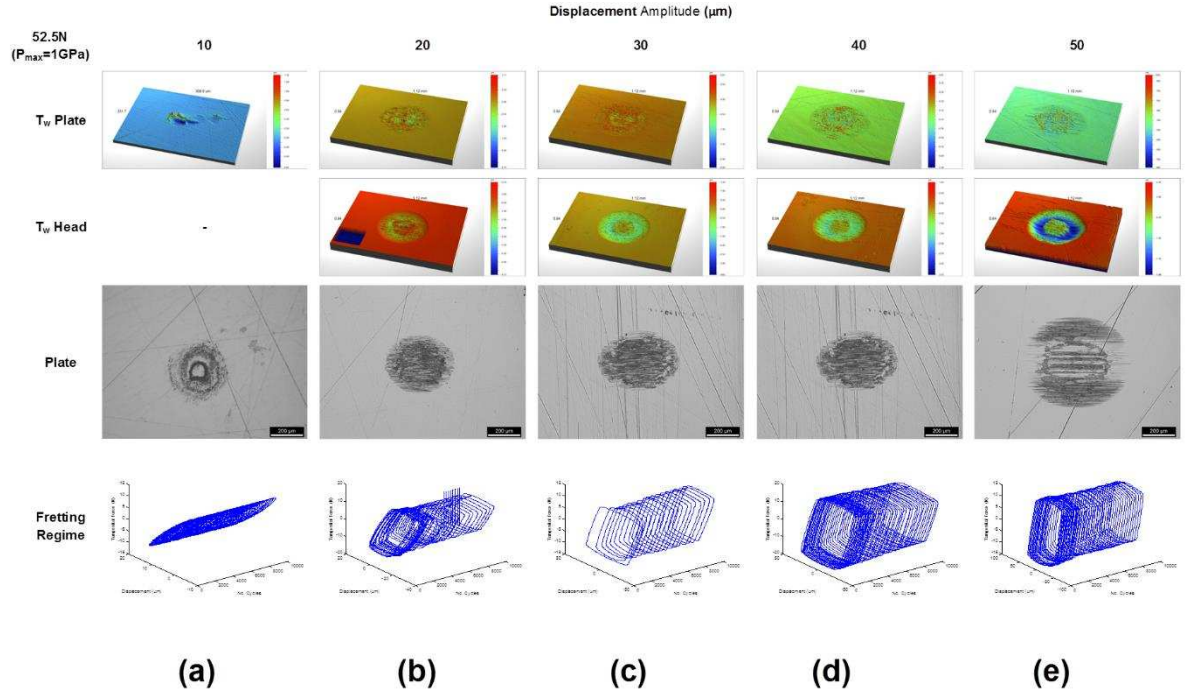

Fig. 4 Fretting observations at P_{max}=1 GPa and δ_d from 10 to 50μm. The transition from partial slip (a), mixed (b) and gross slip regime (c-e) can be observed. T_w represents VSI images for the plate and balls. The combination of these images represents the total weight lost (T_w) during fretting.

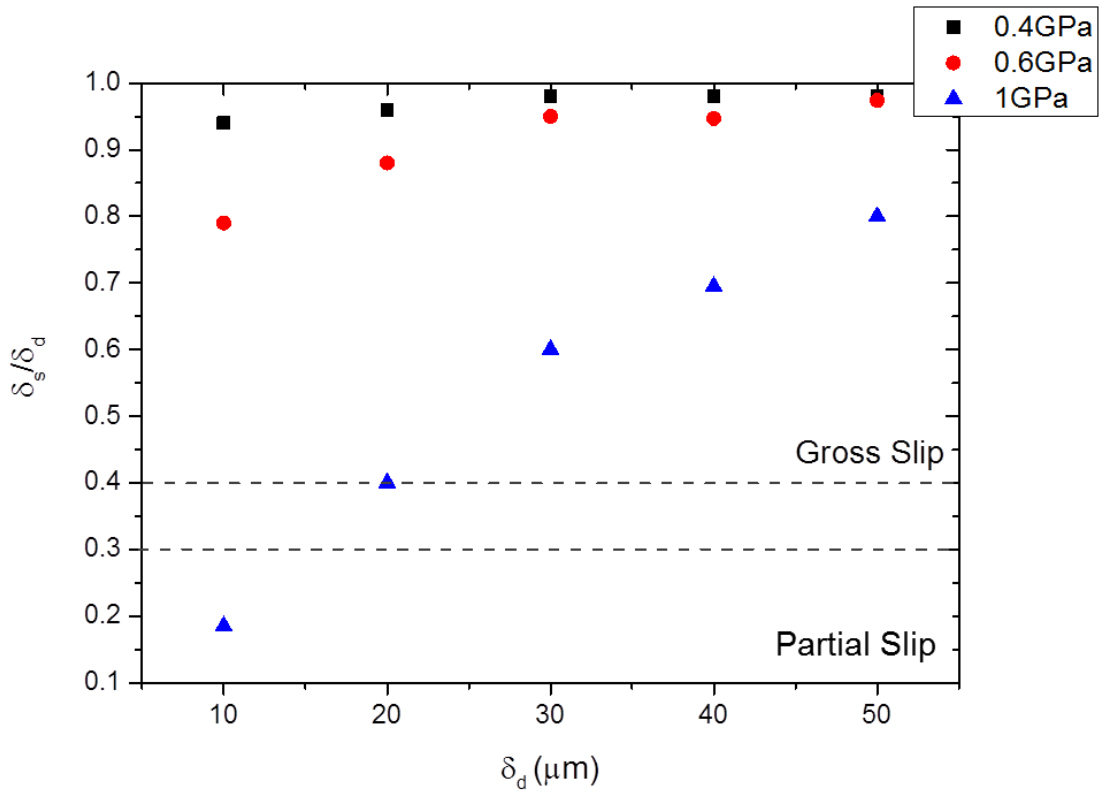

Fig. 5 $\delta_s/\ \delta_d$ as a function of δ_d and contact pressure for CoCr fretting couples. Dashed lines represent the transition from partial to gross slip regimes.

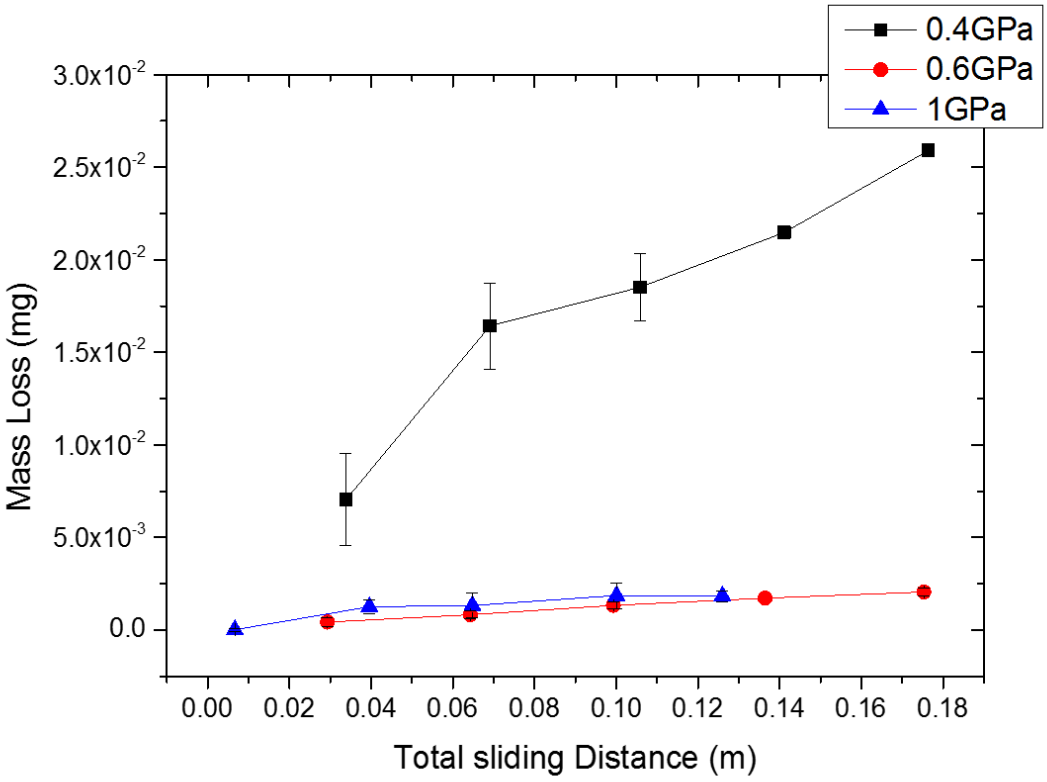

Fig. 6 Total mass loss from the fretting system as a function of actual total sliding distance at the interface.

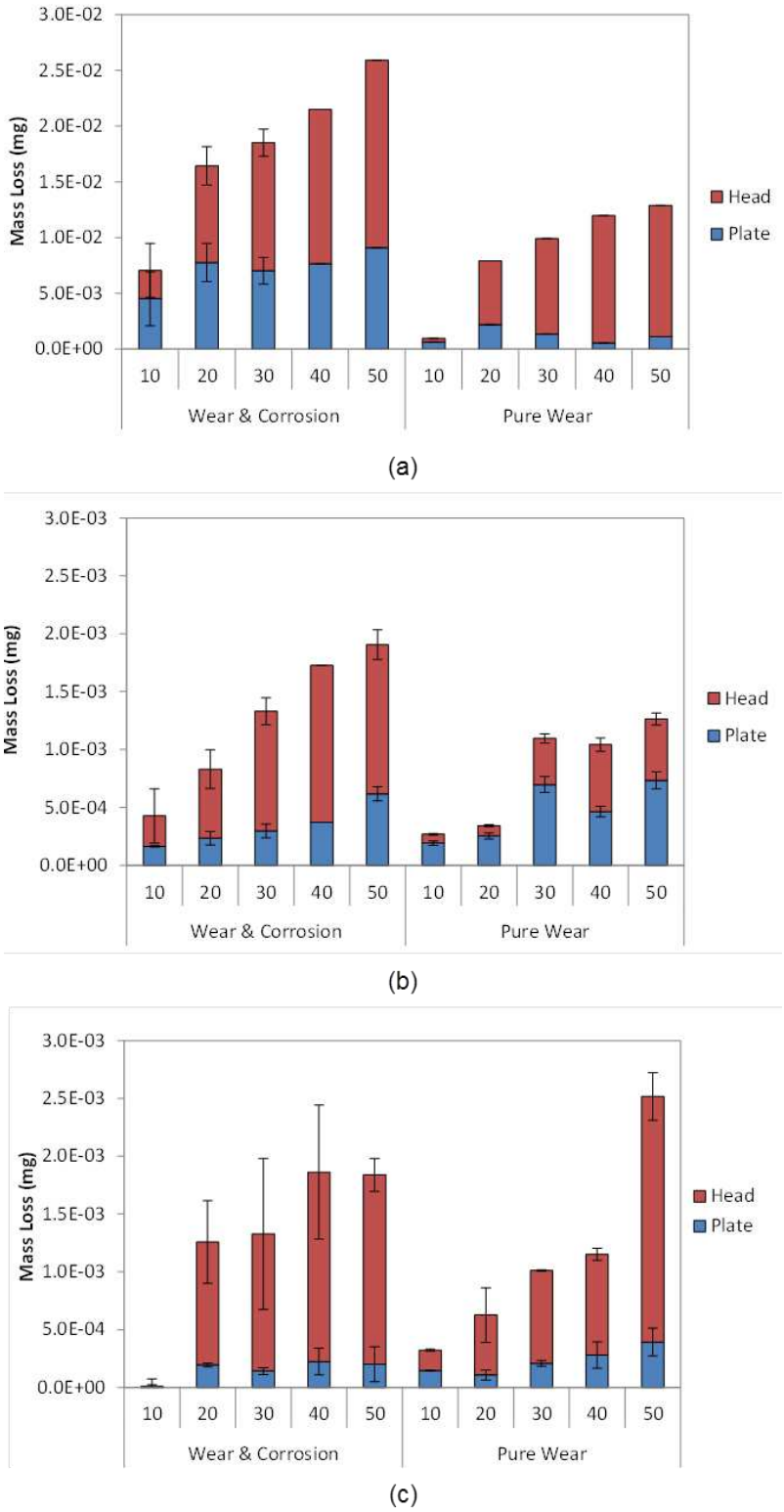

Fig. 7 Total mass loss under equilibrium (wear and corrosion) and pure wear conditions at a) 0.4 GPa b) 0.6 GPa and c) 1 GPa for 10 to 50 µm displacements. Note the order of magnitude between tests conducted at 0.4 GPa and0.6 GPa and 1 GPa.

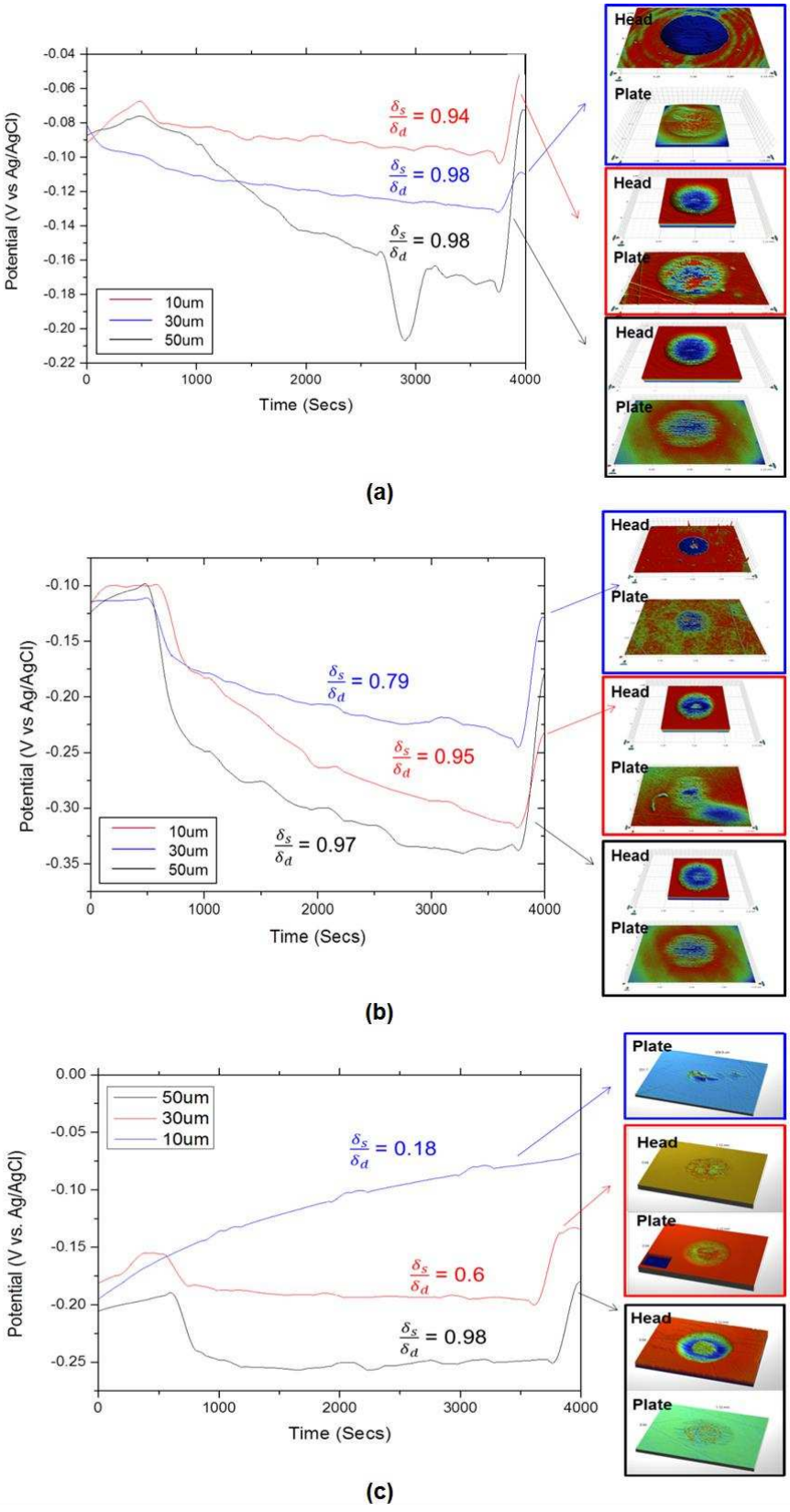

Fig. 8 E_{corr} vs Time for CoCr contacts at a) 0.4 GPa b) 0.6 GPa and c) 1GPa.

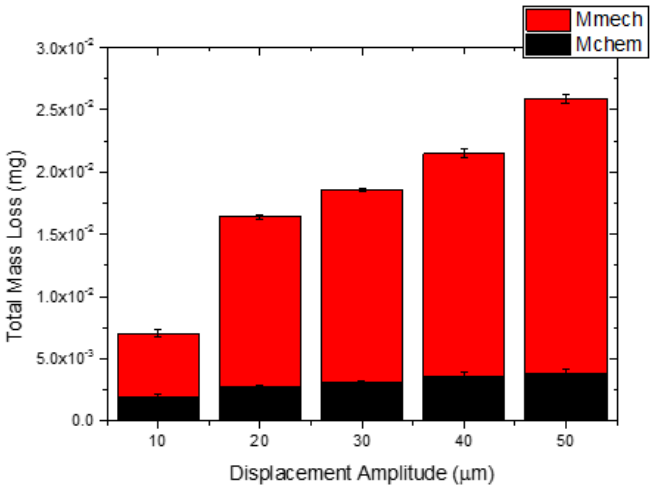

(a)

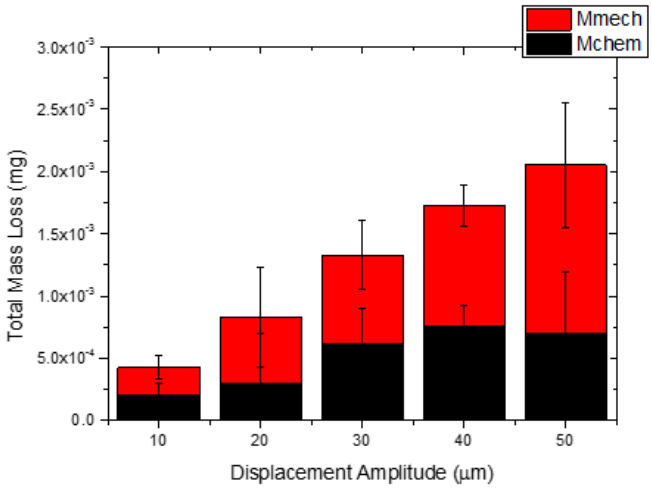

(b)

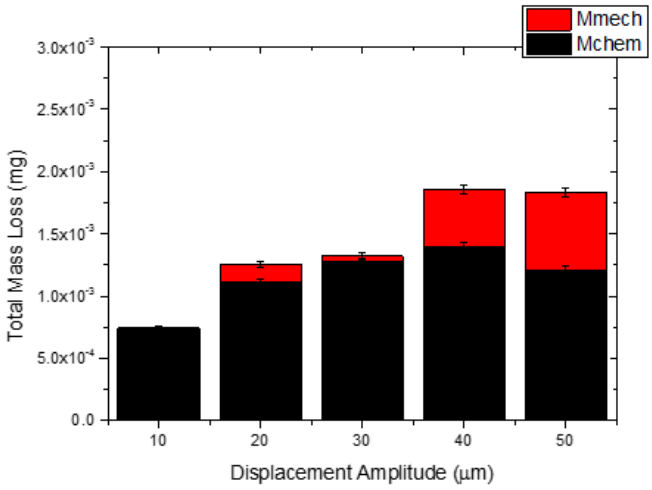

(c)

Fig. 9 Contributors to total mass for CoCr fretting-corrosion contacts at a) 0.4 GPa b) 0.6 GPa and c) 1GPa.

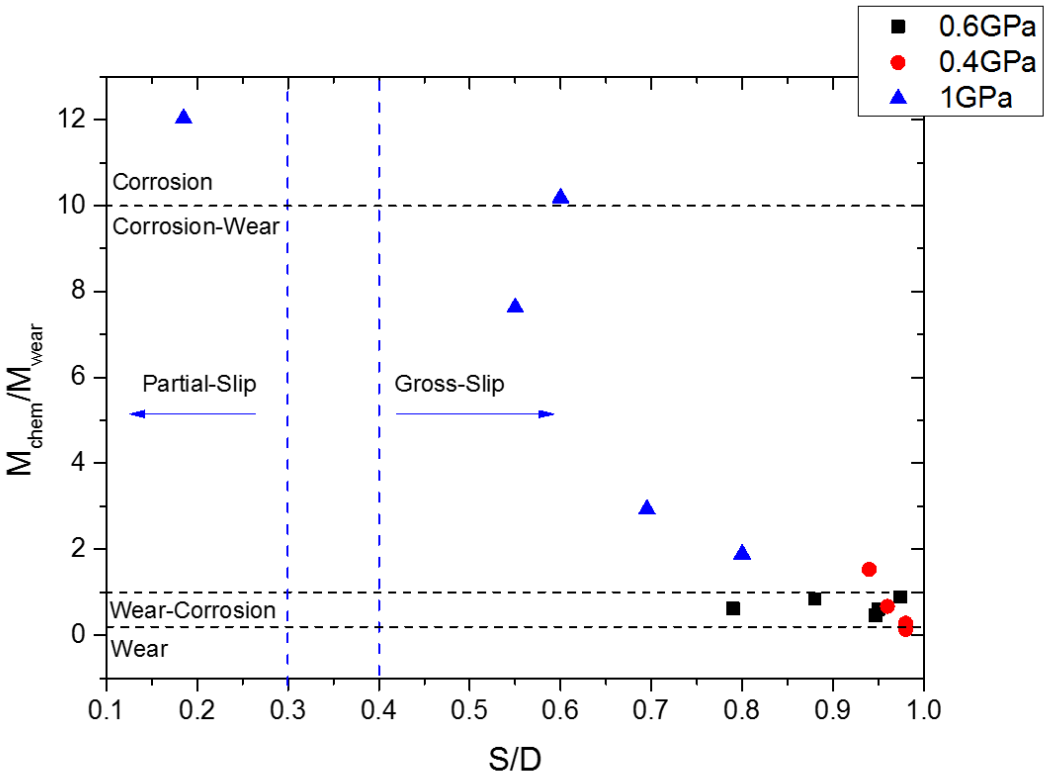

Fig. 10 Dominant degradation mechanism as a function of $\delta_s/\ \delta_d$ and contact pressure.

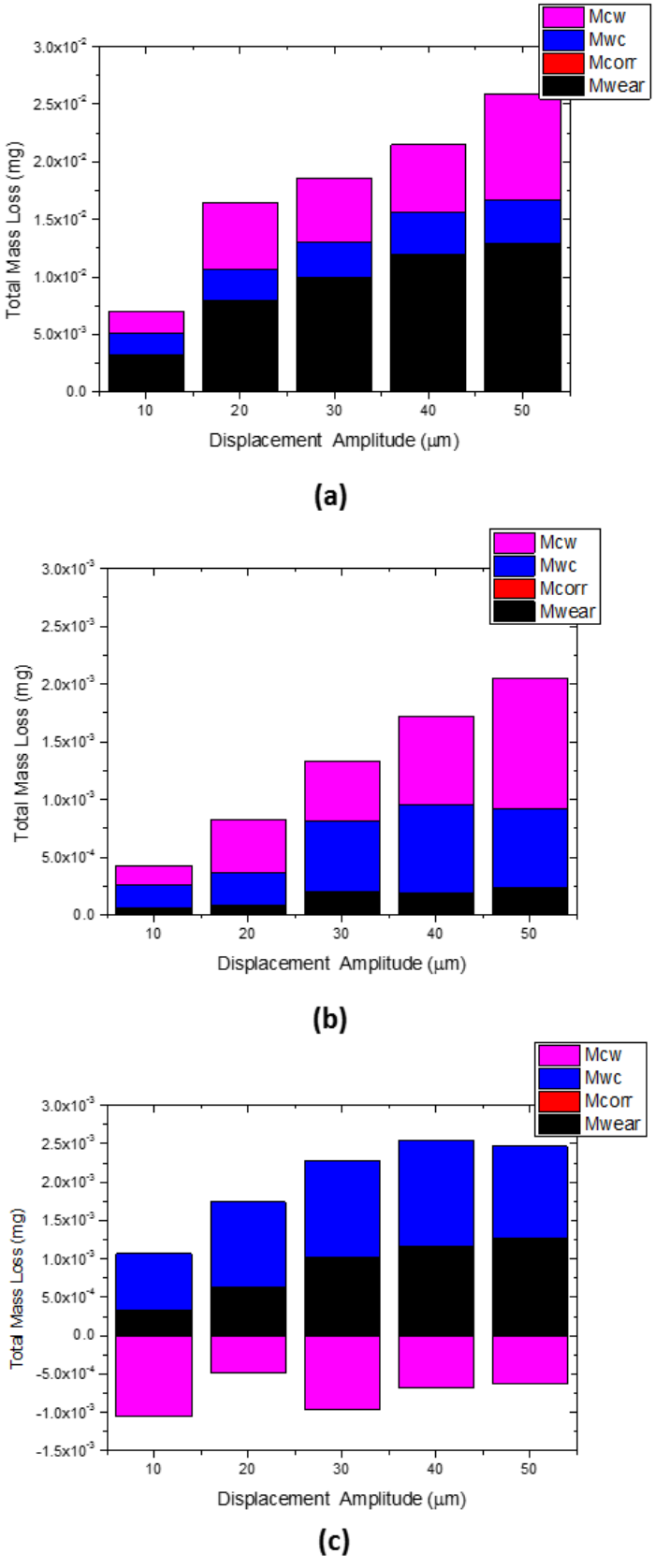

Fig. 11 Breakdown of synergistic terms as given in Eq 1.2 at a) 0.4, b) 0.6 and c) 1GPa.

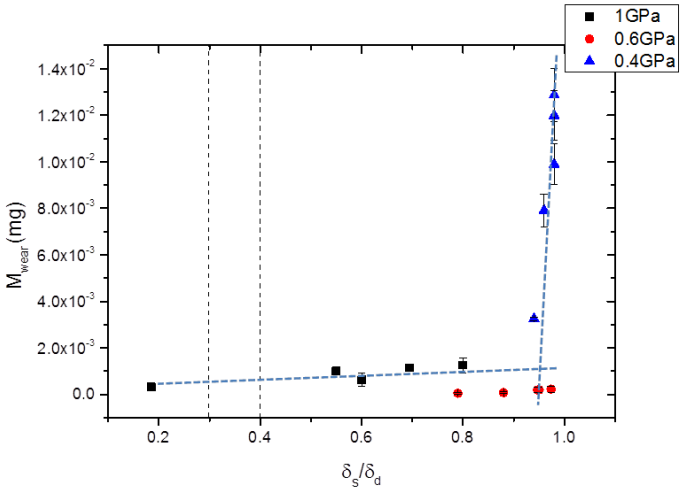
1GPa
0.6GPa
0.4GPa
M_{wear} (mg)
δ_s/δ_d

(a)

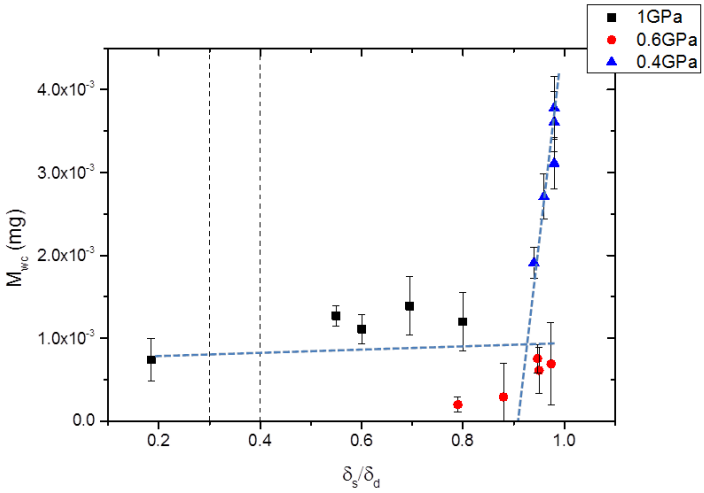
1GPa
0.6GPa
0.4GPa
M_{WC} (mg)
δ_s/δ_d

(b)

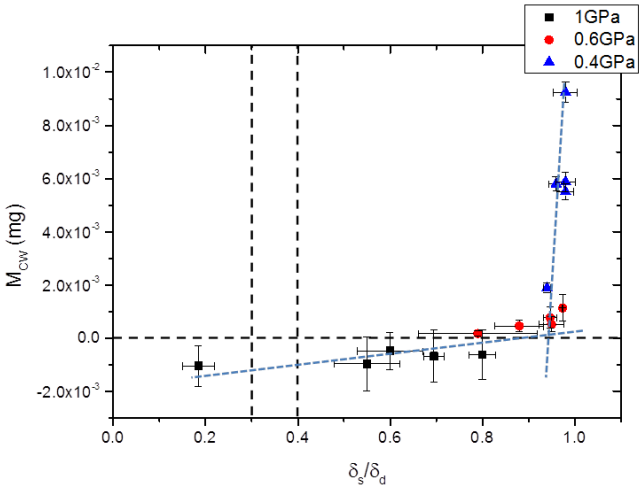
1GPa
0.6GPa
0.4GPa
M_{CW} (mg)
δ_s/δ_d

(c)

Fig. 12 Transition of (a) pure wear (M_{wear}), (b) wear enhanced corrosion (M_{wc}) and (c) corrosion enhanced wear (M_{cw}) for CoCr-CoCr contact as a function of contact pressure and δ_s/δ_d. Dashed lines represent transition criteria used throughout this study.